Journal of the Korean Society for Nondestructive Testing
Vol. 27, No. 3 (2007. 6)

Determination of Incident Angle and Position of Optimal Mode Ultrasonic Beam for Flaw Detection in Anisotropic and Inhomogeneous Weldments by Ray Tracing

Xinyu Zhao*, Sung-Jin Song**,†, Hak-Joon Kim**, Tie Gang*

Suk-Chull Kang***, Yong Hwan Choi***, Kyungcho Kim*** and Sung-Sik Kang***

Abstract Ultrasonic inspection of austenitic steel weldments is a truly difficult task due to complicated wave propagation phenomena such as beam skewing, splitting and distortion. In order to understand these phenomena and design proper inspection procedures, simulation is increasingly paid more attention to. This article addresses a ray tracing based approach to determine incident angle and position of optimal wave mode ultrasonic beam for flaw detection in anisotropic and inhomogeneous austenitic steel weldments. Specially, the optimal mode of ultrasonic wave wave is selected by ray tracing simulation, and an optimization approach based on ray tracing and bi-section search is proposed in order to find the ray path connecting two given points in weldments. With help of this approach, the optimal incident angle and position of ultrasonic beam can be determined for a given flaw position.

Keywords: Ray Tracing, Ultrasound, Austenitic Stainless Steel, Anisotropic, Inhomogenous, Weldment

1. Introduction

Austenitic steel is widely used in many industries due to its high corrosive resistance and excellent creep properties over a range of temperature. However, coarse and oriented grains in weldments often occur during welding procedures. In general, the grain size in any austenitic stainless steel weld is ranging from 0.5 mm to 2.0 mm (Palaniappan and Subbaratnam, 2003). Thus, it is a difficult challenge for ultrasonic inspection of these kind materials due to primarily two factors: one is high attenuation and noise caused by course grains, and the other is beam skewing due to both anisotropic and inhomogeneous elastic media of structures. Anisotropy is usually caused by the grain size, which is large relative to the ultrasonic wavelength, and inhomogeneity is caused by the significant variation in grain orientation through the weldment (Ogilvy, 1988).

In order to address such difficulty in ultrasonic inspection of austenitic steel weldments, research works have been carried out for describing the material properties and its effects on ultrasonic wave propagation. Several modeling methods, such as ray tracing (Ogilvy, 1985), multi-Gaussian beam model (Spies, 2000) and finite element methods (Apfel et al., 2005) have been developed to predict the beam

Received: April 16, 2007, Accepted: May 25, 2007. * State Key Laboratory of Advanced Welding Production Technology, Harbin Institute of Technology, Harbin 150001, China, ** School of Mechanical Engineering, Sungkyunkwan University, 300 Chunchun-dong, Jangan-gu, Suwon, Kyunggi-do 440-746, Korea, *** Korea Institute of Nuclear Safety, Daejeon 305-338, Korea, † Corresponding author: sjsong@skku.edu

propagation and ultrasonic field distribution.

This paper proposes an optimization approach for selecting optimized inspection parameters such as ultrasonic wave mode, and beam incident angle and position for flaw detection in anisotropic and inhomogeneous weldments. For this purpose, an austenitic weld structure model proposed by Ogilvy (Ogilvy, 1985) is considered as a sample problem. Then ray tracing procedure is briefly discussed since it is a crucial tool for design optimization of ultrasonic inspection. Then several ray tracing results are given for the selection of the optimal wave mode. Finally, two examples are given in which optimal incident angle and position are determined for a given flaw location in the austenitic weldments.

2. Description of Austenitic Weldments

2.1 Grain Orientation

Coarse and oriented grains in austenitic weld are mainly governed by three physical phenomena: epitaxial growth, influence of temperature gradient, and selective growth (Moysan et al., 2003). In the case of austenitic multi-pass welds, when a new weld pass is given, only a thin layer gets recrystallization in the previous pass according to special thermal conditions, and then epitaxial growth easily occurs, which leads the grain to follow the crystalline orientation of the previous pass. In this way, the grain grows up through several welded layers keeping approximately the same direction within rather large areas (Chassignole et al., 2000a). Another important phenomenon is that the grains, whose $<100>$ direction parallel to the temperature gradient direction, grow up fastest and hence stifle the growth of unsuitably oriented grains. The result of this selective growth is that there is a strong consistency between the orientation of columnar grain in weld metal and the $<100>$ crystallographic axes of individual crystals.

2.2 Elastic property

It has been appreciated that austenitic steel weld metal is anisotropic, and much work has been done to characterize the elastic anisotropy using all kinds of method such as ultrasonic measurement and X-ray diffraction measurement (Chassignole et al., 2000b). The elastic property of grain with oriented texture in austenitic steel weld can be described as transversely isotropic, which has five independent elastic constants. The elastic constants of transversely isotropic are given with respect to a crystal coordinate (sometimes called material coordinate system) in a contracted index notation as,

$$C_{IJ} = \begin{pmatrix} C_{11} & C_{12} & C_{13} & & & \\ & C_{11} & C_{13} & & & \\ & & C_{33} & & & \\ & & & C_{44} & & \\ & sym & & & C_{44} & \\ & & & & & \frac{(C_{11}-C_{12})}{2} \end{pmatrix}$$

2.3 Modeling Austenitic Weld Structure

Although the austenitic steel weld has complicated anisotropy and inhomogeneity, some rules also have been found. Firstly, for general weld structure, the columnar grain only tilted in the plane perpendicular to the weld direction, and not tilted out of this plane. Secondly, the grain orientations keep approximately constant along the sloping face at each side of the weld, but slightly tilted in the middle of the weld. And the slope of grain axis decreases with increasing distance from the centre of the weld. According to such regularities, models to describe the structure of austenitic stainless steel weld were developed by several scholars (Apfel et al., 2005). Ogilvy defined a mathematic function, given by eqn.(1), which describes well the grain structure of V-butt welds. The detail descriptions on the parameters in this function can be found in reference (Ogilvy, 1985).

$$F(y,z)=\begin{cases}\tan\theta_1=\dfrac{T_1(D_1+z\tan\alpha_1)}{y^n} & y>0\\ \tan\theta_2=\dfrac{T_2(D_2+z\tan\alpha_2)}{y^n} & y<0\end{cases} \quad (1)$$

Only the welding seam is the effective zone of the function, and the base metal is regarded as isotropic ferrite steel. One example of the calculated results using Ogilvy grain structure model is shown in Fig. 1.

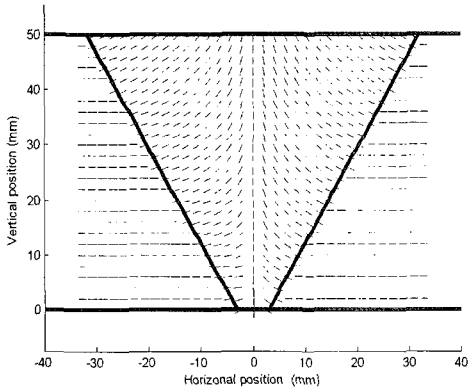

Fig. 1 A plot of grain orientations in weld

3. Wave Propagation Fundamentals in Anisotropic Media

3.1 Slowness and Group Velocity

In this section we outline the governing equations for waves propagating in an anisotropic elastic solid and demonstrate the important roles that the slowness and group velocity play in these problems. Since these are well-known, it is just to describe them here briefly. When dealing with reflection and refraction problem it is convenient to rewrite Christoffel's equation in a different form as,

$$(C_{ijkl}s_j s_k-\rho\delta_{il})d_l=0 \quad (2)$$

where C_{jikl} is the elastic constants, ρ is the density, $\vec{d}=d_i\hat{e}_i$ is the polarization vector, and $\vec{s}=(1/v)\vec{l}$ defines the slowness vector (inverse velocity). The slowness depends on the propagation direction $\vec{l}$, we solve eqn. (2) for a given propagation direction and that direction will then be varied to map out a complete slowness surface.

Handling with anisotropic media it is important to discuss another velocity called the group velocity. The group velocity is determined mathematically by

$$g=\frac{\partial\omega}{\partial k_i}\underset{\sim}{e}_i=\frac{\partial v}{\partial l_i}\underset{\sim}{e}_i \quad (3)$$

We can use the definition of the group velocity to obtain,

$$g_j=\frac{1}{\rho}C_{ijkl}s_k d_l d_i \quad (4)$$

The group velocity will be used to determine the direction of energy flow.

3.2 Reflection and Refraction of Waves at an Interface between two Anisotropic Media

Consider a plane wave incident from upper grain to the boundary between zones with different grain orientation (as shown in Fig. 2). In general, the incident wave transforms on the boundary into three reflected and three refracted waves. Then according to continuity of displacement and stress, the boundary conditions can be written as,

$$\begin{cases}u_{I,i}^{\gamma}+\sum\limits_{\alpha=qP,qS1,qS2}u_{R,i}^{\alpha}=\sum\limits_{\beta=qP,qS1,qS2}u_{T,i}^{\beta}\\ \sigma_{I;i3}^{\gamma}+\sum\limits_{\alpha=qP,qS1,qS2}\sigma_{R;i3}^{\alpha}=\sum\limits_{\beta=qP,qS1,qS2}\sigma_{T;i3}^{\beta}\quad i=1,2,3\end{cases} \quad (5)$$

where u_i are the displacement components and the stress components for the wave of type are given by

$$\begin{aligned}\sigma_{i3}^{\alpha}&=i\omega D_i^{\alpha}U^{\alpha}e^{ik_m^{\alpha}x_m}\\ D_i^{\alpha}&=C_{i3kl}s_k^{\alpha}d_l^{\alpha}\end{aligned} \quad (6)$$

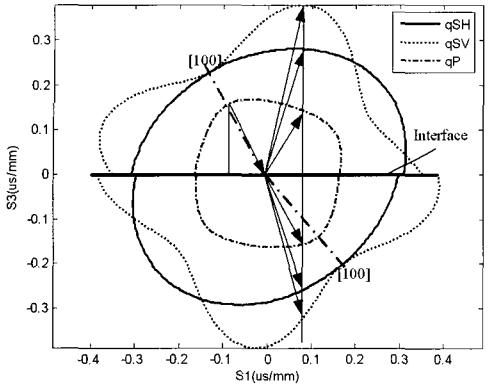

Fig. 2 Reflection and refraction at the boundary between zones with different grain orientation

In eqn. (5) the superscripts α,β,γ are the wave types, and the subscripts I, R and T denote the incident, reflected and transmitted waves, respectively.

For harmonic plane waves, the phase match must be satisfied in the system of six equations (eqn. (5)). Then it can be shown that the frequencies of all the reflected and refracted waves must be equal to the incident wave frequency. And it also can be shown that all the slowness vectors lie in the same incident plane and have the same projection onto the boundary as the incident wave (which is acquired by Snell's law). Thus, if the interface coordinate system is selected the slowness components for the reflected and refracted waves $s_2^{\alpha}(\alpha = qP, qSH, qSV)$ is zero, and s_1^{α} is equal to the incident slowness component s_1^{i} which is known, then only slowness component which is left to be determined is the s_3^{α}. To find s_3^{α} the Christoffel's equation (eqn. (2)) needs to set,

$$\left|C_{ijkl}s_j s_k - \rho\delta_{il}\right| = 0 \tag{7}$$

which can be expanded to a sixth order equation for s_3^{α} since $s_3^{\alpha} = 0$ and s_1^{α} is known. For a given s_1^{α}, six solutions can be found in the anisotropic medium as shown in Fig. 3. In order to choose three physical roots (which may be real or complex) from the six solutions, the group velocity should be examined for the real roots, and the complex solutions must lead to an exponential decay of the amplitude with distance from the interface (Henneke II, 1972).

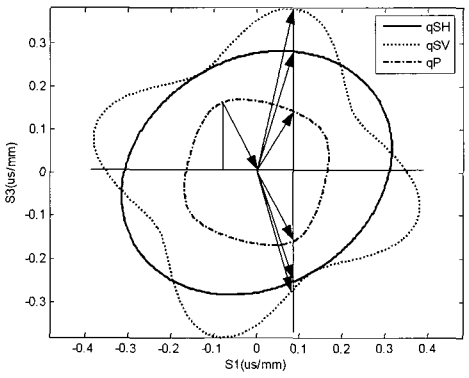

Fig. 3 Six solutions for a given incident angle

4. Ray Tracing

4.1 Ray Tracing Algorithm

A ray tracing method that has been originally developed by Ogilvy (Ogilvy, 1985) can find the tracing paths of ultrasound through weldments which include regions of anisotropic and inhomogeneous materials. The algorithm used in the present work is quite similar to Ogilvy's, however, it is not exactly the same. It can be summarized as follows,

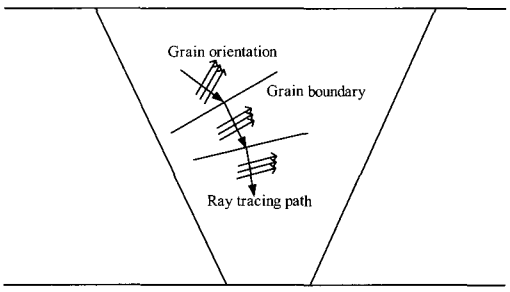

Fig. 4 Schematic representation of ray tracing

1. Find the grain orientation of the current ray position and assume the local crystal orientation is the same as that of the current ray point.
2. Determine a vector representing one half difference of gain orientation between the current point and the point on which the previous calculation has been performed. Treat this as the artificial grain boundary. Then transform the stiffness tensor from the material coordinates to the current interface coordinates.
3. Solve eqn. (7) in the current interface coordinates to get the refracted slowness of the same wave type in term of the previous position slowness direction and the elastic tensor of the current position.
4. Calculate the refracted group velocity using the new slowness direction and the corresponding polarizations in the interface coordinates according to eqn. (4). Then transform the slowness and group velocities from the interface coordinates to the specimen coordinates. Move one step forward in the group velocity direction from the grain boundary to next position.
5. Return to the step 1 and repeat until the fixed ray's length is reached.

It has to mention that the problem of what kind artificial interface should be selected cannot be explained theoretically, different interfaces were also be used in the other paper (Schmitz et al., 1999).

4.2 Simulation Results

In this section we will show some ray tracing results which are similar to those of Ogilvy (Ogilvy, 1985 and Ogilvy, 1988). The purpose of this simulation is of two aspects; firstly to provide an evidence of the accuracy of the present work, and secondly and more importantly, to select the optimal mode of ultrasonic beam to be used for inspecting austenitic steel welds.

Fig. 5 shows the predictions of ray paths from three wave modes with transducer normal incident at the different positions. Due to the symmetry of grain structure model in weld, we just display the rays in a half weld part. Obviously, the difference with the isotropic media can be found from the calculated results. The curve propagation paths in anisotropic and inhomogeneous weld lead to difficulty to evaluate positions of flaws. By comparison of three different wave modes, the pattern of qSH seems more adequate for inspecting austenitic steel welds, and the qSV mode would be hard due to disturbed ray paths. These behaviors were caused by the dramatic changes of slowness curvature for the qSV wave, while smooth changes for qSH mode.

Since it is difficult to excite and receive the qSH mode wave in practice, the qP mode was paid more attention for practical inspection of austenitic steel welds. The predictions of ray paths of qP wave modes with 45° oblique incident was shown in Fig. 6. It suggests better scanning inspection when angle beam transducers

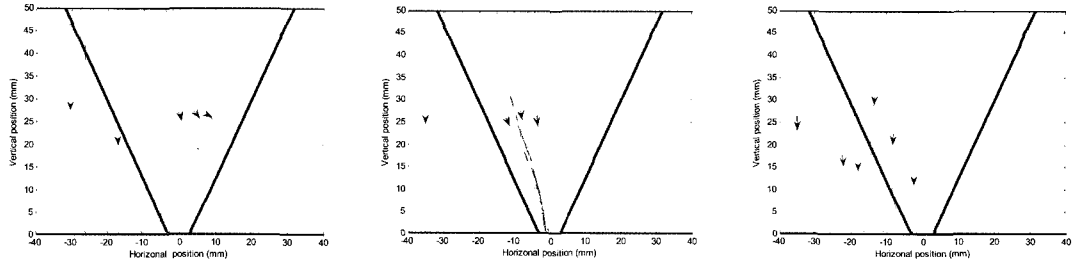

(a) qP wave normal incident (b) qSV wave normal incident (c) qSH wave normal incident

Fig. 5 Simulation of normal incident beam propagation for three mode waves

were used. So, the qP wave is selected as an optimal mode and used in the following section of the paper.

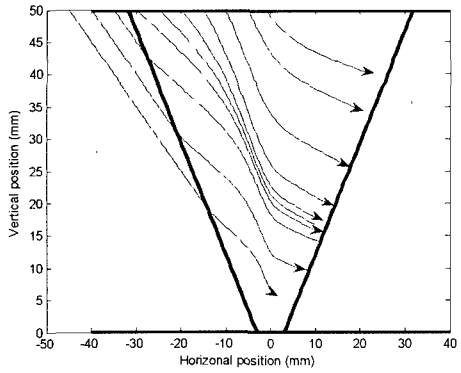

Fig. 6 qP wave 45°oblique incident

5. Optimization of Inspecting Parameter

In this study, an optimization approach based on ray tracing and bi-section search is proposed in order to find the ray path connecting two given points in weldments. Specifically, two practical cases are considered as follows.

5.1 Determination of Incidence Angle

As shown in Fig. 7, a planar transducer which is mounted on a Lucite wedge is considered, and the star means the flaw location in weldment. If the transducer position is fixed, one has to choose an incident angle that satisfies the ray propagating through the flaw location. Thus, the following procedure is developed to solve such a problem. First, calculate the incident angle which satisfies the ray propagating through

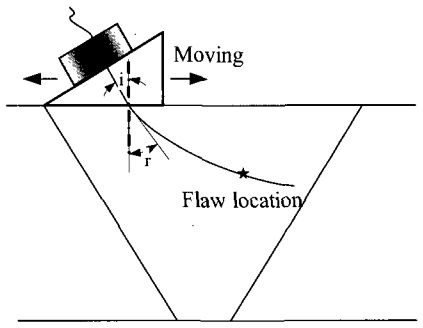

Fig. 7 Schematic representation for an optimizational approach

the given point with an assumption of homogeneous and isotropic medium. Treat this angle as the first input value for austenitic weldment case and calculate the ray trace. Second, if the calculated ray trace path is below/above the given point, then increase/decrease the incident angle and calculate again. Finally, since the low and top limits have been set a priori, the bisectional search is repeatedly used to seek the ray path that meets the certain accuracy criterion. Here, the minimum distance between the ray path and the fixed point is selected as a standard for adjustment. Since the step size of ray tracing is 0.5 mm, so if the minimum distance is less than 0.5 mm, one can consider the ray path is close enough to the flaw location, then stop searching. The process of searching for the optimized incident angle lists in Table 1. And Fig. 8 (a) shows the calculated ray tracing paths for a fixed transducer location. The optimized incident angle of 22.10° is for a fixed transducer position of (-40,50) and a flaw location of (0,25).

Table 1 Searching optimized incident angle

n	θ_i	$\mathbf{x}_i$	$\mathbf{x}_f$	$\mathbf{x}$	$\lvert\mathbf{x}_f - \mathbf{x}\rvert$
1	23.27	(-40,50)	(0, 25)	(-0.02, 30.07)	5.09
2	21.27			(-2.94, 24.76)	3.18
3	22.27			(0.28, 25.47)	0.742
4	21.77			(-1.26, 24.78)	1.4867
5	22.10			(-0.14, 24.77)	0.3761

5.2 Determination of incident location

The other practical case is that, for a fixed angle transducer and a given flaw location in weldment, one has to determine the transducer position that can make sure the ray passing through the flaw location. The procedure for this case is similar to the above-mentioned one. First, calculate an initial incident position with an assumption of isotropic, homogeneous medium and find the ray path from this initial location. Then, if the calculated ray trace is on the left/right side of the given point, then move the incident position to right/left until determination of both low and top limits. Finally, seek the ray path meeting certain accuracy standard by dichotomizing search. As shown in Fig. 8(b), the optimized transducer location of (32.17, 50) is determined for a 45° angled transducer and a flaw location of (0, 20). And the process of searching for the optimized incident position lists in Table 2.

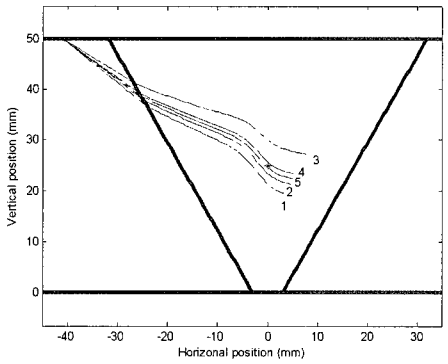

(a) Seeking suitable incident angle for a fixed incident point

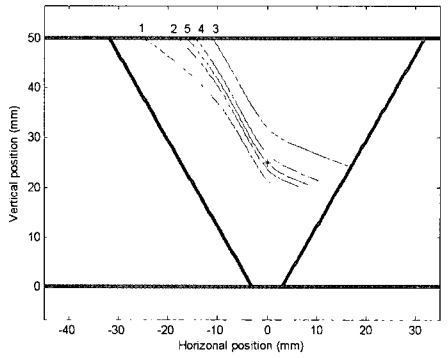

(b) Seeking suitable incident point for a fixed incident angle

Fig. 8 Determination of optimized inspection parameters for tow different cases

6. Conclusion

In this paper, the main ideas of ray tracing method were overviewed. By comparing the calculated ray paths and some practical considerations, the qP wave is selected as an optimal wave mode to be used in practical inspection with angle transducers. Then an optimization approach based on ray tracing and bi-section search was established in order to select optimized inspection parameters (such as incident angle and location) for a given flaw location. Simulation results presented in this paper demonstrate that the optimization approach proposed in the present work can serve as a practical tool to search suitable inspection parameters for austenitic steel weldments.

Table 2 Searching optimized incident position

n	$\mathbf{x}_i$	θ_r	$\mathbf{x}_f$	$\mathbf{x}$	$\lvert\mathbf{x}_f - \mathbf{x}\rvert$
1	(-25,50)	45°	(0, 25)	(-6.18, 20.62)	10.56
2	(-18,50)			(-0.93, 24.88)	1.04
3	(-11, 50)			(0.32, 31.76)	7.08
4	(-14.5,50)			(0.38,26.35)	1.73
5	(-16.25,50)			(0.05, 24.91)	0.14

References

Apfel, A., Moysan, J., Corneloup,G., Fouquent, T. Chassignole, B. (2005) Coupling an Ultrasonic Propagation Code with a Model of the Heterogeneity of Multi-Pass Welds to Simulate Ultrasonic Testing, Ultrasonics, Vol. 43, pp. 447-456

Chassignole, B., Villard, D., Nguyen Van Chi, G., Grnhrmbre, N. Lhemery, A. (2000a) Ultrasonic Propagation in Austenitic Stainless Steel Welds Approximate Model and Numerical Methods Results and Comparison with Experiments, D. O. Thompson and D. E. Chimenti (Eds.), *Review of Progress in Quantitative Nondestructive Evaluation*, Vol. 20, AIP, New York, pp. 153-160

Chassignole, B., Villard, D., Dubuget, M., Babous, J-C. El Guerjouma, R. (2000b) Characterization of austenitic stainless steel welds for ultrasonic NDT, D.O. Thompson and D.E.Chimenti (Eds.), *Review of Progress in Quantitative Nondestructive Evaluation*, AIP, New York, Vol. 20, pp. 1325 1332

Henneke II, E.G. (1972) Reflection-Refraction of a Stress Wave at a Plane Boundary Between Anisotropic Media, J. Acoust. Soc. Am. Vol. 51, pp. 210-217

Moysan, J., Apfel, A., Corneloup, G. and Chassignole, B. (2003) Modelling the grain orientation of austenitic stainless steel multipass welds to improve ultrasonic assessment of structural integrity, International Journal of Pressure Vessels and Piping Vol. 80, pp. 77 85

Ogilvy, J. A. (1985) Computerized Ultrasonic Tay Tracing in Austenitic Steel, NDT & E International, Vol. 18, pp. 67-77

Ogilvy, J. A. (1988) Ultrasonic Reflection Properties of Planar Defects within Austenitic Welds, Ultrasonics, Vol. 26, pp. 318-327

Palaniappan, M. and Subbaratnam, R. (2003) Ultrasonic Examination of Thick Austenitic Stainless Steel Welds and Factors Influence the Sensitivity, Journal of Korean Society for Nondestructive Testing, Vol. 23, pp. 372-379

Schmitz, V., Walte, F. and Chakhlov, S. V. (1999) 3D Ray Tracing in Austenite Materials, NDT & E International, Vol. 32, pp. 201-213

Spies, M. (2000) Modeling of Transducer Fields in Inhomogeneous Anisotropic Materials Using Gaussian Beam Superposition, NDT & E International, Vol. 33, pp. 155-162